A chemoproteomic platform to quantitatively map targets of lipid-derived electrophiles

Chu Wang[1,2], Eranthie Weerapana[1,2], Megan M Blewett[1,2] & Benjamin F Cravatt[1,2]

Cells produce electrophilic products with the potential to modify and affect the function of proteins. Chemoproteomic methods have provided a means to qualitatively inventory proteins targeted by endogenous electrophiles; however, ascertaining the potency and specificity of these reactions to identify the sites in the proteome that are most sensitive to electrophilic modification requires more quantitative methods. Here we describe a competitive activity–based profiling method for quantifying the reactivity of electrophilic compounds against >1,000 cysteines in parallel in the human proteome. Using this approach, we identified a select set of proteins that constitute 'hot spots' for modification by various lipid-derived electrophiles, including the oxidative stress product 4-hydroxy-2-nonenal (HNE). We show that one of these proteins, ZAK kinase, is labeled by HNE on a conserved, active site–proximal cysteine and that the resulting enzyme inhibition creates a negative feedback mechanism that can suppress the activation of JNK pathways normally induced by oxidative stress.

The functional diversity of mammalian proteomes is enriched by the post-translational modification of proteins[1]. Many such modifications are enzyme catalyzed, but others reflect the direct (non-enzymatic) oxidative or electrophilic modification of nucleophilic residues, such as cysteine, by reactive small molecules that are often the products of oxidative stress[2,3]. Chronic inflammation or hypoxia, for instance, induces the peroxidation of polyunsaturated lipids to generate a broad range of electrophilic products[2]. These lipid-derived electrophiles (LDEs) can modify DNA and proteins to promote cytotoxicity and have been implicated in the pathogenesis of many diseases[4]. A growing body of studies also suggests that, at lower, more physiologically standard concentrations, LDEs serve as endogenous messengers that modulate the response of signaling pathways[5,6]. HNE, for instance, is a major product generated when free radicals initiate the non-enzymatic fragmentation of lipids in biological membranes[2,7]. The levels of HNE and HNE-protein adducts are elevated in cells and tissues exposed to oxidative stress, and HNE can regulate redox-responsive signaling pathways by mechanisms that are still poorly understood[2,8,9]. 15-Deoxy-Δ12,14-prostaglandin J2 (15d-PGJ2) is another LDE produced by a set of enzymes that metabolize arachidonic acid[10]. 15d-PGJ2 exhibits anti-inflammatory and cytoprotective properties and has therefore been designated as a pro-resolving signal[10]. A third example is 2-*trans*-hexadecenal (2-HD), which is a product of sphingolipid metabolism and has recently been shown to function as a protein-modifying cofactor that promotes mitochondrial pathways for apoptosis[11].

Understanding the protein targets of LDEs is critical for elucidating their cellular functions and mechanisms of action. Chemoproteomic methods have proven particularly useful for inventorying a large number of proteins that react with LDEs in cells and tissues[2,12–17]; however, quantifying the potency and specificity of these reactions to identify the sites in the proteome that are most sensitive to electrophilic modification has proven challenging. Here we describe a competitive activity–based protein profiling (ABPP) method for quantifying the reactivity of electrophilic compounds against >1,000 cysteines in parallel in the human proteome. Using this approach, we identified select sets of proteins that are preferentially modified by HNE and 15d-PGJ2. We show that the kinase ZAK is labeled by HNE on a conserved, active site–proximal cysteine residue, which inhibits the enzyme and suppresses the activation of JNK pathways by oxidative stress in cancer cells.

RESULTS

Quantitative proteomic profiling of LDE-cysteine reactions

Among the 20 protein-coding amino acids, cysteine is unique owing to its high nucleophilicity, which renders it sensitive to modification by endogenous and exogenous electrophiles and oxidants[3]. Cysteine reactions with electrophilic metabolites have been characterized for purified proteins[18,19] and, on a global scale, in cells and tissues using mass spectrometry–based chemoproteomic[2,12–17] and imaging methods[20]. These studies—along with analytical, quantum mechanical and kinetic work[21,22]—have, for the most part, confirmed the preferential reactivity that Michael acceptor electrophiles such as HNE show for cysteine over other nucleophilic amino acids (for example, lysine or histidine) in proteomes. We were interested in building on these past findings to determine whether individual cysteines in the proteome display differences in their reactivity with LDEs and, if so, whether potential hot spots for electrophile modification might constitute key nodes in signaling pathways of redox sensing and response.

[1]The Skaggs Institute for Chemical Biology, The Scripps Research Institute, La Jolla, California, USA. [2]Department of Chemical Physiology, The Scripps Research Institute, La Jolla, California, USA. Correspondence should be addressed to C.W. (chuwang@scripps.edu) or B.F.C. (cravatt@scripps.edu).

RECEIVED 23 APRIL; ACCEPTED 11 OCTOBER; PUBLISHED ONLINE 1 DECEMBER 2013; DOI:10.1038/NMETH.2759

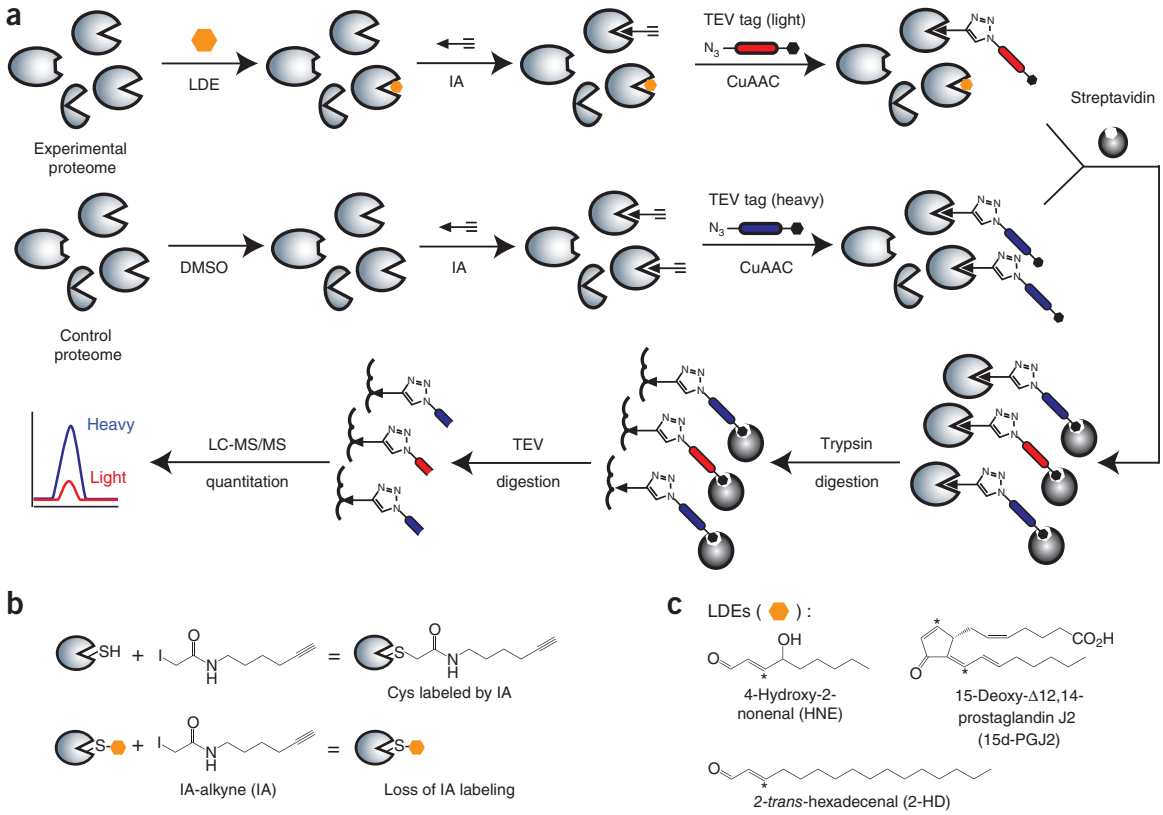

Figure 1 | Competitive isoTOP-ABPP for quantitative mapping of cysteine–lipid-derived electrophile (LDE) reactions in proteomes. (**a**) Competitive isoTOP-ABPP involves treatment of proteomes with DMSO or LDE, proteome labeling with an IA-alkyne (IA) probe, CuAAC-based incorporation of isotopically labeled, tobacco etch virus (TEV) protease–cleavable biotin tags, enrichment with streptavidin and sequential on-bead protease digestions to afford probe-labeled peptides for liquid chromatography–tandem mass spectrometry (LC-MS/MS) analysis. (**b**) Structures of the IA probe and the competitive blockade of IA-cysteine reactions by an LDE. (**c**) Structures of three LDEs—HNE, 15d-PGJ2 and 2-HD—used in competitive isoTOP-ABPP experiments, with their sites of reactivity marked by asterisks.

We previously described a chemoproteomic method termed isotopic tandem orthogonal proteolysis–ABPP (isoTOP-ABPP) and its use to quantify the intrinsic reactivity of cysteine residues in cell and tissue proteomes[23]. Here we envisioned that isoTOP-ABPP could be advanced to discover and quantify reactions between cysteines and electrophilic small molecules in proteomes. In this 'competitive' version of isoTOP-ABPP (**Fig. 1a**,**b**), a proteome is treated with an electrophile (experimental sample) or dimethyl sulfoxide (DMSO; control sample). Both proteomic samples are then labeled with an alkynylated iodoacetamide (IA) probe (**Fig. 1b**) and conjugated by copper-catalyzed azide-alkyne cycloaddition (CuAAC, or 'click'[24]) chemistry to light and heavy azide-biotin tags, respectively, each containing a tobacco etch virus (TEV) cleavage sequence. The light and heavy samples are then mixed and subjected to our described isoTOP-ABPP protocol for peptide enrichment, cleavage and identification, in which IA-modified cysteines are identified and their extent of labeling quantified according to mass spectrometry MS2 and MS1 profiles, respectively[23]. Electrophile-sensitive cysteines are quantified by measuring the MS1 chromatographic peak ratios (*R* values) for heavy (DMSO-treated) over light (electrophile-treated) samples, with higher *R* values reflecting greater sensitivity to the electrophile. In this format, competitive isoTOP-ABPP can assay electrophiles against >1,000 cysteines in parallel directly in native proteomes without requiring any chemical modification to the electrophiles themselves.

We applied competitive isoTOP-ABPP to quantitatively profile the proteome reactivity of three LDEs—HNE, 15d-PGJ2 and 2-HD—each of which possesses an α,β–unsaturated carbonyl that can react with nucleophilic cysteines via Michael addition (**Fig. 1c**). Competitive isoTOP-ABPP experiments were performed in quadruplicate using the soluble proteome of the human breast cancer cell line MDA-MB-231. Proteomes were treated with 100 μM of HNE, 15d-PGJ2 or 2-HD for 60 min and then with the IA-probe (100 μM, 60 min). A total of ~1,000 cysteine reactivities were quantified across the aggregate data set, with at least 750 cysteine reactivities quantified for each LDE (**Fig. 2a**), more than 550 of which were quantified for all the three LDEs (**Supplementary Fig. 1** and **Supplementary Table 1**). Most of the cysteine reactivities (>98%) were unaffected or only marginally affected by LDE treatment ($R < 5$); however, a select subgroup showed marked reductions in their IA-probe reactivities ($R > 5$) following exposure to one or more LDEs (**Fig. 2a**). HNE and 15d-PGJ2 both targeted several cysteines in the proteome, the majority of which showed preferential reactivity with one of the two LDEs, whereas 2-HD exhibited no detectable high-sensitivity ($R > 5$) targets (**Fig. 2a**). We also analyzed LDEs in a second human cancer cell proteome (Ramos cells), which increased our proteome coverage (>900 cysteines reactivities quantified for all three LDEs) and revealed good overall correlation of reactivity profiles compared to MDA-MB-231 proteomes (**Supplementary Fig. 2**).

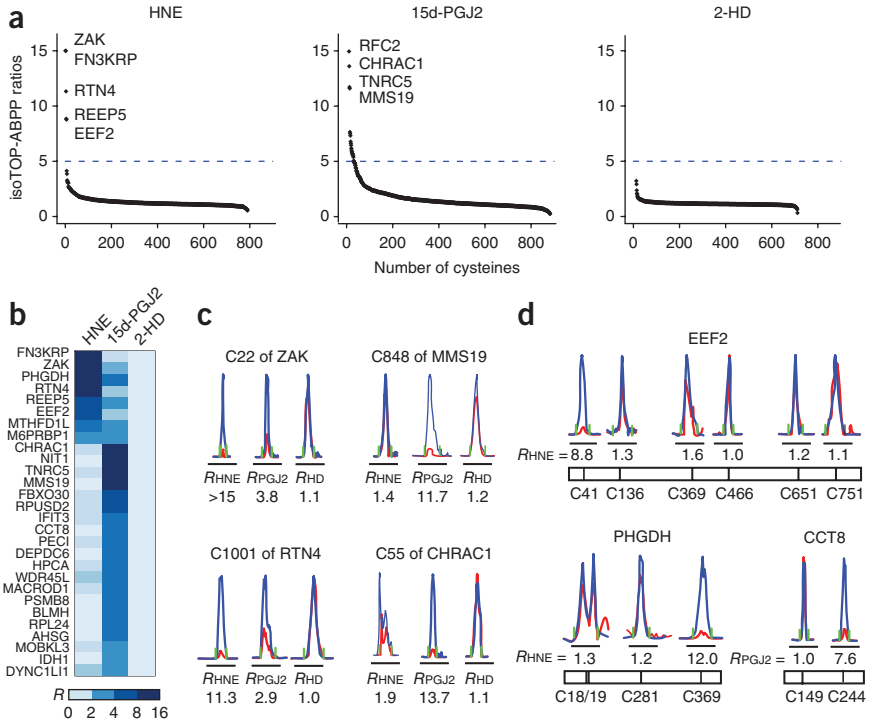

Figure 2 | Quantitative profiling of LDE-cysteine reactions in proteomes. (**a**) Distribution of competitive isoTOP-ABPP ratios (*R* values) quantified from reactions with the human MDA-MB-231 proteome treated with 100 µM HNE (five technical replicates from four biological replicates), 15d-PGJ2 (six technical replicates from five biological replicates) or 2-HD (four technical replicates from three biological replicates). A cutoff of fivefold or greater blockade of IA-probe labeling (*R* values >5) is shown by dashed lines to mark cysteines that exhibit high sensitivity to LDEs, and proteins with cysteines showing the strongest competitive reactivity with LDEs are labeled by names. (**b**) Heat map of cysteines with *R* values >5, illustrating examples of cysteines that display selectivity for reacting with one of the three tested LDEs. (**c**) Representative MS1 profiles for peptides containing cysteines that show selective competition with HNE (left) or 15d-PGJ2 (right). Heavy (untreated) and light (LDE-treated) traces are colored in blue and red, respectively. Green lines mark boundaries of integrated peak areas for quantitation. (**d**) Representative MS1 profiles for multiple cysteine–containing peptides from the same protein, only one of which shows sensitivity to LDE competition.

The quantitative ranking of cysteines based on the magnitude and selectivity of their inhibition illuminated hot spots for LDE reactivity in the proteome (**Fig. 2a**,**b**, **Supplementary Table 2** and **Supplementary Fig. 2**). Examples included Cys22 of ZAK and Cys848 of MMS19, which were strongly and selectively blocked by HNE and 15d-PGJ2, respectively (**Fig. 2c**). Competitive isoTOP-ABPP also identified several proteins that possess multiple IA-reactive cysteines, only one of which proved sensitive to competitive blockade by an LDE (**Fig. 2d**). These data demonstrate that the quantified *R* values reflect measurements of individual LDE-cysteine reactions rather than general changes in protein abundance potentially caused by LDE exposure. We also found that LDE-sensitive cysteines spanned a broad range of intrinsic reactivity (**Supplementary Fig. 3**), as determined previously by measuring their extents and rates of IA labeling[23], a result suggesting that their modification by LDEs depends not only on cysteine nucleophilicity but also on molecular recognition of the LDEs.

Determining the potency of HNE-cysteine reactions

We next focused on identifying the most sensitive sites for LDE reactivity in the proteome. The MDA-MB-231 cell proteome was treated with varying concentrations of HNE (5, 10, 50, 100 and 500 µM) for 60 min, and then the IA labeling profile of each reaction was quantitatively compared to a DMSO-treated control sample by isoTOP-ABPP. By combining the *R* values at all five HNE concentrations, we could extrapolate the half-maximal inhibitory concentrations, or IC_{50} values, for HNE blockade of IA-probe labeling for ~700 of the ~1,100 total cysteines detected in the study (**Fig. 3a** and **Supplementary Table 3**). This analysis revealed that the vast majority of cysteines were

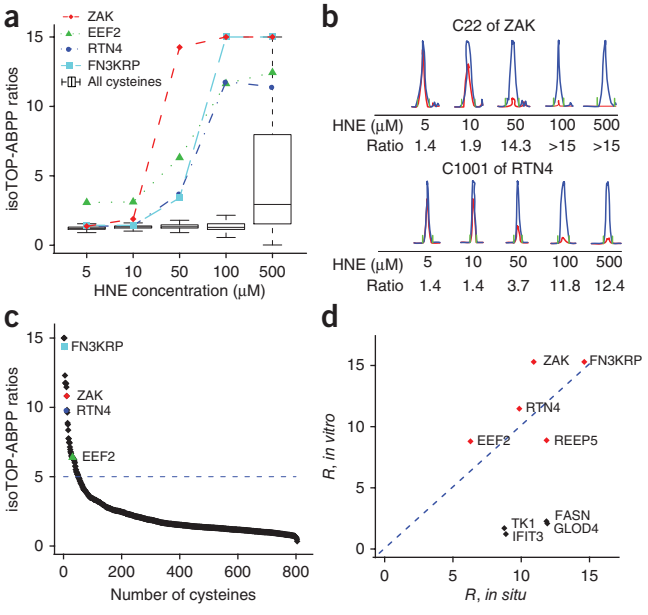

Figure 3 | Determining the potency of HNE-cysteine reactions in proteomes and in cells. (**a**) Box plots (maximum, 1.5× the interquartile range) showing the distribution of *R* values for ~1,100 cysteines quantified from competitive isoTOP-ABPP experiments with the MDA-MB-231 proteome treated with 5, 10, 50, 100 and 500 µM HNE, in comparison with the *R* values quantified for cysteines from ZAK, EEF2, RTN4 and FN3KRP. The data reported here are representative of an experiment run in duplicate. (**b**) Representative MS1 profiles for HNE-sensitive cysteines in ZAK and RTN4 showing concentration-dependent blockade of IA labeling by HNE. (**c**) Distribution of *R* values quantified from competitive isoTOP-ABPP experiments with proteomes from MDA-MB-231 cells treated *in situ* with DMSO or HNE (100 µM, 60 min; two biological replicates). (**d**) Comparison of *R* values obtained from *in vitro* versus *in situ* competitive isoTOP-ABPP experiments. Diamond color indicates whether cysteines show similar (red) or different (black) *in vitro* and *in situ* *R* values.

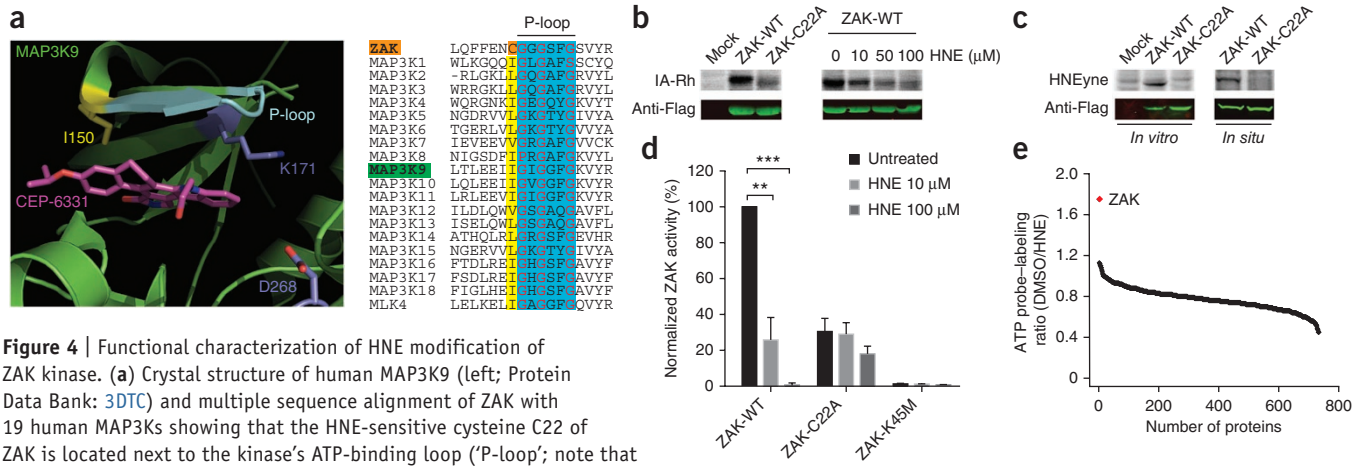

Figure 4 | Functional characterization of HNE modification of ZAK kinase. (**a**) Crystal structure of human MAP3K9 (left; Protein Data Bank: 3DTC) and multiple sequence alignment of ZAK with 19 human MAP3Ks showing that the HNE-sensitive cysteine C22 of ZAK is located next to the kinase's ATP-binding loop ('P-loop'; note that C22 corresponds to I150 in MAP3K9) and is unique to ZAK among other MAP3K enzymes. (**b**) Selective IA labeling of wild-type (WT) but not C22A ZAK and concentration-dependent competition of IA labeling of WT ZAK by HNE as measured by gel-based ABPP using an IA-rhodamine (IA-Rh) probe. Flag-tagged ZAK proteins were expressed in HEK-293T cells by stable transfection and immunoprecipitated before IA-probe labeling and analysis. (**c**) An HNE-alkyne probe (HNEyne[12]) selectively labels WT but not C22A ZAK in proteomes and in living cells as determined by gel-based ABPP. For **b** and **c**, the experiments were repeated three times with consistent results (not shown). (**d**) Catalytic activity of immunoprecipitated WT but not C22A ZAK is inhibited by HNE as measured with a myelin basic protein–substrate assay. A K45M ZAK mutant, in which a conserved active-site lysine was mutated, showed no detectable activity and thus served as a catalytically dead control enzyme. All three ZAK variants (WT, C22A and K45M) were expressed at similar levels in transfected HEK-293T cells (**Supplementary Fig. 4**). Data are presented as mean values ± s.e.m.; $n = 3$ experiments per group. $^{**}P = 0.004$, $^{***}P = 2 \times 10^{-7}$, *t*-test, two sided. (**e**) SILAC-ABPP of acyl phosphate–ATP probe reactivity for ZAK-transfected HEK-293T cell proteomes pretreated with DMSO (heavy cell proteome) or HNE (light cell proteome; 100 μM, 30 min).

modified by HNE with low potency (IC_{50} values > 100 μM), but a select few cysteines, including Cys22 of ZAK, Cys41 of EEF2, Cys24 of FN3KRP and Cys1001 of RTN4, exhibited much higher sensitivities with IC_{50} values ranging from 6 to 23 μM (**Fig. 3a**,**b**). We next confirmed that these hypersensitive cysteines were also inhibited by HNE *in situ* by treating MDA-MB-231 cells with 50 or 100 μM HNE and then preparing proteomes for analysis by competitive isoTOP-ABPP (**Fig. 3c**,**d** and **Supplementary Table 4**). Another set of cysteines showed reductions in IA-probe labeling *in situ* but not *in vitro* (**Fig. 3d**). This finding suggests that certain proteins may preferentially react with HNE in living cells, although we cannot exclude, at this point, that the reductions in IA-probe labeling observed for these proteins reflect a decrease in their overall abundance in HNE-treated cells.

Functional analysis of HNE modification of ZAK kinase

ZAK kinase (also known as MLK7 or MLTK) functions as a mitogen-activated kinase kinase kinase (MAP3K) that can activate all three major MAPK (ERK, JNK and p38) pathways in mammalian cells[25–27], with some preference for JNK[26], and is involved in responding to stressors such as UV radiation[28] and chemotherapeutic agents[27]. Sequence and structure comparisons allowed us to map the HNE-sensitive cysteine in ZAK (C22) to a location proximal to the glycine-rich ATP-binding loop ('P-loop') (**Fig. 4a**). Interestingly, among all 20 human MAP3Ks, ZAK is the only member that possesses a cysteine at this position (**Fig. 4a**), and this cysteine is highly conserved across ZAK orthologs in vertebrates (**Supplementary Fig. 4**). This information, combined with the high sensitivity displayed by Cys22 for HNE (**Fig. 3a**) motivated us to further characterize this interaction and its impact on ZAK activity.

We first expressed Flag-tagged versions of wild type (WT) and a C22A mutant of ZAK by stable transfection in HEK-293T cells and found that WT ZAK showed much stronger IA-rhodamine–probe labeling as measured by gel-based ABPP. The IA-rhodamine labeling of WT ZAK was blocked by pretreatment with HNE over a concentration range that closely matched the HNE-sensitivity profile observed for Cys22 in competitive isoTOP-ABPP experiments (**Fig. 4b**; compare to **Fig. 3a**). We next used an alkyne-functionalized HNE probe (HNEyne)[12] to verify that WT ZAK was directly labeled, and that the C22A ZAK mutant was not, *in vitro* and in living cells (**Fig. 4c**). HNE also inhibited WT but not C22A ZAK activity in a concentration-dependent manner, as measured with an *in vitro* myelin basic protein (MBP) substrate assay[29] (**Fig. 4d**). We note that C22A ZAK exhibited reduced basal activity compared to WT ZAK, but the residual activity of C22A ZAK, which was still much greater than a catalytically dead K45M ZAK mutant, was insensitive to HNE (**Fig. 4d** and **Supplementary Fig. 5**). Considering that Cys22 is predicted to reside adjacent to the ATP-binding loop of ZAK, we postulated that the HNE-induced loss of kinase activity might be due to blockade of ATP binding. We tested this hypothesis by performing a competitive stable-isotope labeling by amino acids in cell culture (SILAC)-ABPP[30] experiment using an acyl phosphate–ATP probe[31], which revealed that probe labeling of ZAK, but not of other proteins, was substantially reduced in cell proteomes treated with HNE (**Fig. 4e**).

HNE modification of ZAK suppresses JNK activation in cells

We next evaluated the activation state of MAPK signaling pathways in HEK-293T cells stably expressing WT ZAK, C22A ZAK or K45M ZAK. WT ZAK–expressing cells, but not C22A or K45M ZAK–expressing cells, showed increased JNK and, to a lesser extent, p38 and ERK pathway activation compared to mock-transfected cells, as measured by anti-phosphoprotein blotting (**Fig. 5a**,**b** and **Supplementary Fig. 6**). We next treated cells with H_2O_2 (1 mM, 30 min) to induce oxidative stress, a process that is known to activate the JNK pathway[32]. H_2O_2 treatment stimulated JNK activity in both WT and C22A ZAK–transfected cells (but not K45M ZAK–transfected cells), with WT-ZAK cells showing

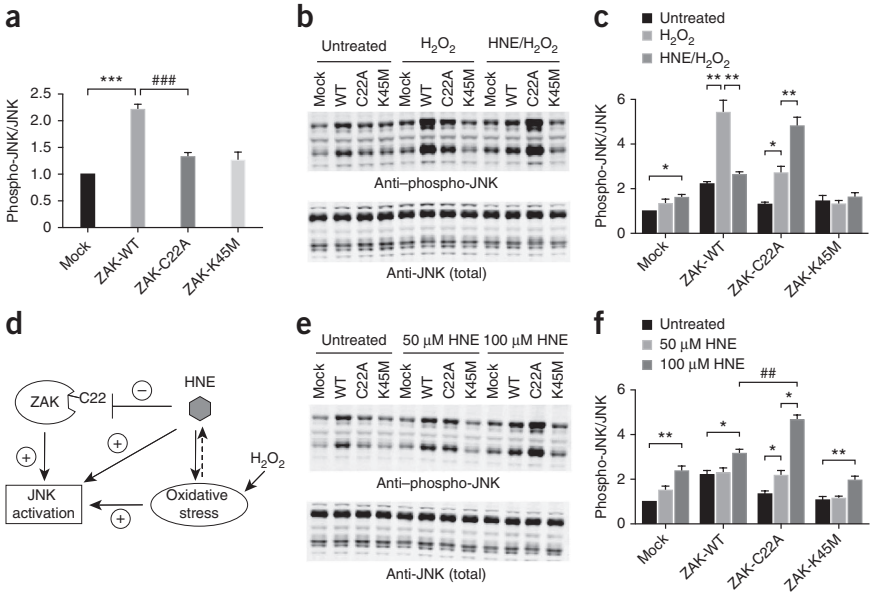

Figure 5 | HNE modification of ZAK suppresses JNK pathway activation in cells. (**a**) WT ZAK–transfected HEK-293T cells show higher basal JNK activation than do mock–, C22A ZAK– or K45M ZAK–transfected cells. Data are presented as mean values ± s.e.m.; $n = 8$; $^{***}P = 7 \times 10^{-9}$; $^{\#\#\#}P = 1 \times 10^{-5}$; *t*-test, two sided. (**b**,**c**) Western blots (**b**) and normalized phosphorylated JNK levels (**c**) of ZAK-transfected cells treated with H_2O_2 (1 mM, 30 min) with or without pretreatment with HNE (100 μM, 30 min). (**d**) Model diagramming ZAK-dependent and ZAK-independent pathways for HNE modulation of JNK activation. Dashed line designates the potential for oxidative stress to generate HNE and initiate a negative feedback loop to limit JNK activation. (**e**,**f**) Western blots (**e**) and normalized phosphorylated JNK levels (**f**) of ZAK-transfected cells treated with HNE (50 or 100 μM, 60 min). For **c** and **f**, data are presented as mean values ± s.e.m.; $n = 4$ experiments per group (biological replicates). $^{*}P < 0.05$; $^{**}P < 0.01$; $^{\#\#}P < 0.01$; *t*-test, two sided. Exact *P* values are provided in **Supplementary Figure 8**.

the greater level of activation (**Fig. 5b**,**c**). Strikingly, however, pretreatment with HNE (100 μM, 30 min) produced opposing effects in WT- and C22A-ZAK cells, blocking H_2O_2-dependent JNK activation in the former cell model and hyperactivating JNK activity in the latter. We interpret these findings to indicate the existence of both ZAK-dependent and ZAK-independent pathways for HNE modulation of JNK activation (**Fig. 5d**). By modifying Cys22 on ZAK, HNE blocks the contribution that this kinase makes to activation of the JNK pathway. HNE is also known to itself promote oxidative stress[33] that likely adds to the effects of H_2O_2 and, in the context of an HNE-resistant C22A ZAK mutant, would serve to further augment activation of the JNK pathway. In this model, the HNE-ZAK interaction acts as a negative feedback loop that tempers activation of the JNK pathway under high and/or persistent levels of oxidative stress (**Fig. 5d**). We further tested this idea by evaluating the effects of HNE alone on JNK pathway activity in ZAK-expressing cells. A dramatic concentration-dependent activation of JNK was observed in C22A-ZAK cells but not in WT-ZAK cells, which showed higher basal JNK activation that was mostly unaffected by HNE (**Fig. 5e**,**f**). Although we were initially surprised that HNE treatment did not appear to block the basal JNK activation caused by WT ZAK, we should note that HNE also activated JNK in mock-transfected cells to a level that matched the basal JNK activity observed in WT ZAK–transfected cells. Thus, the residual JNK activation observed in WT ZAK–transfected cells may reflect ZAK-independent pathways of JNK activation by HNE (**Fig. 5e**,**f**). That JNK activation was much higher in C22A-ZAK cells than in the other cell models indicates this HNE-insensitive form of ZAK, which still retains some catalytic activity (**Fig. 4d**), combines with ZAK-independent, HNE-stimulated pathways to further enhance JNK activation.

DISCUSSION

Long viewed as biomarkers of oxidative damage, LDEs have more recently gained attention as second messengers that can regulate diverse cellular processes[5,34]. Considering that the signaling and pathophysiological functions of LDEs may differ across the endogenous concentration ranges found for these compounds, it is imperative to understand the potencies of LDE-protein interactions in biological systems. With this goal in mind, we created a competitive isoTOP-ABPP platform to quantitatively map LDE-reactivity across >1,000 cysteines in parallel, resulting in the discovery of discrete sites of hypersensitivity, or hot spots, for LDE modification in the human proteome.

Among the most LDE-sensitive cysteines, Cys22 of ZAK captured our interest because of the proposed role of this kinase in activating JNK, ERK and p38 MAPK pathways in both cancer[25] and inflammation[27]. To date, only a handful of studies have investigated ZAK function, and its modes of regulation remain poorly understood. That HNE inhibits human ZAK by modifying an active site–proximal cysteine conserved among ZAK orthologs, but not other MAP3K enzymes, suggests that ZAK acts as a special node in MAPK signaling pathways that confers sensitivity to lipid oxidation products. In this way, HNE modification of ZAK may limit the extent of JNK activation caused by oxidative stress, which could help certain cell types, such as tumor and immune cells, survive in the presence of high levels of reactive oxygen species. Further studies of ZAK function would benefit from the development of selective inhibitors for this enzyme. It is noteworthy, in this regard, that covalent inhibitors targeting active-site cysteine residues have recently been introduced for many kinases[35], leading us to speculate that the Cys22-HNE interaction discovered herein may offer a medicinal chemistry starting point for the development of ZAK inhibitors. Beyond ZAK, we also identified several other kinases in our competitive isoTOP-ABPP experiments that possess cysteines inhibited by HNE, albeit with lower potencies (**Supplementary Table 5**). Prominent among these was cysteine (Cys311) in AKT1/2/3, which is an active site–proximal residue implicated in substrate binding[36] and was inhibited by HNE with an IC_{50} value of ~60 μM (**Supplementary Table 3**). These proteomic findings confirm recent work showing that recombinant AKT2 is modified by HNE on Cys311 (ref. 18).

We believe that competitive isoTOP-ABPP offers several advantages over more conventional proteomic approaches for the discovery and characterization of protein–small molecule reactions in biological systems. First, quantitative inhibition values are measured in relative terms that are independent of absolute protein abundance. The method is therefore able to sift through signals that span a broad range of intensities to identify reactive sites that are more likely to bear functional consequence. Here the site specificity afforded by isoTOP-ABPP is important because it permits the discovery of potent electrophile-cysteine reactions that may occur on proteins that display other unaffected and/or nonfunctional cysteines (**Fig. 2d**). Endogenous electrophiles also vary considerably in their structures and the stability of the protein adducts that they form. These features can complicate the direct detection of electrophile-protein interactions in proteomics studies. By competitively assessing electrophile-protein interactions using a structurally simple IA probe that forms stable adducts with cysteines, isoTOP-ABPP affords a robust and uniform way to detect and quantify cysteine-electrophile adducts in proteomes by mass spectrometry. The method should also prove applicable to profiling electrophile-protein reactions in primary cells and/or tissues[23], as isotopic tags are conveniently appended to these adducts by click chemistry.

There are, however, some potential shortcomings of competitive isoTOP-ABPP. Because this method indirectly identifies sites of electrophile action by competitive displacement, it remains possible that, in certain instances, blockade of IA-probe labeling could be due to electrophile modification of a neighboring residue rather than the IA-labeled cysteine itself. We addressed this potential concern for ZAK by follow-up studies using a clickable HNE probe[12], which labeled WT ZAK but not a C22A ZAK mutant. We envision that a similar strategy could be used to confirm additional LDE-cysteine interactions discovered in competitive isoTOP-ABPP experiments. Competitive isoTOP-ABPP may also fail to detect certain electrophile-cysteine reactions that occur on very low–abundance proteins or on nonproteotypic peptides incompatible with mass spectrometric detection. Alternative protease digestion protocols should prove capable of identifying at least a subset of these electrophile-cysteine reactions. We should further note that, although the potency of LDE-cysteine reactions is likely important for proteins that are inhibited by LDEs in cells, this parameter may be less relevant for LDE-cysteine reactions that stimulate protein function[2,9]. Indeed, only a modest level of LDE modification may be needed to activate some signaling pathways such as, for instance, the HNE-mediated induction of the heat-shock response by modifying heat-shock proteins to release bound HSF1 (refs. 2,9). We identified several lower-potency, IA-reactive cysteines in Hsp90 (**Supplementary Fig. 7**), and it is possible that one or more of these HNE-cysteine reactions contributes to disrupting Hsp90-HSF1 interactions. Finally, natural electrophiles are also known to target amino acids beyond cysteine[14,37], and these reactions could be quantitatively profiled by adapting competitive isoTOP-ABPP to map other nucleophilic amino acids in proteomes. For this, the continued exploration of simple reactive groups that preferentially and stably modify specific amino acid side chains in proteins is warranted[38,39].

METHODS

Methods and any associated references are available in the online version of the paper.

Note: Any Supplementary Information and Source Data files are available in the online version of the paper.

ACKNOWLEDGMENTS

We thank K. Backus, D. Bachovchin, B. Lanning, K. Tsuboi and A. Adibekian from the Cravatt Lab for providing reagents, and the Marletta lab at The Scripps Research Institute for sharing instrumentation for data collection. This work was supported by the US National Institutes of Health (NIH) (CA087660), an NIH/NIEHS K99/R00 Pathways to Independence Postdoctoral Award (K99ES020851, C.W.), a Pfizer Postdoctoral Fellowship (E.W.), a US National Science Foundation predoctoral fellowship (M.M.B.) and the Skaggs Institute for Chemical Biology.

AUTHOR CONTRIBUTIONS

B.F.C., C.W. and E.W. conceived of the project. C.W., E.W. and M.M.B. performed experiments. B.F.C. and C.W. analyzed data and wrote the manuscript.

COMPETING FINANCIAL INTERESTS

The authors declare no competing financial interests.

1. Walsh, C.T. *Posttranslational Modification of Proteins: Expanding Nature's Inventory* (Roberts & Company, 2005).
2. Jacobs, A.T. & Marnett, L.J. Systems analysis of protein modification and cellular responses induced by electrophile stress. *Acc. Chem. Res.* **43**, 673–683 (2010).
3. Leonard, S.E. & Carroll, K.S. Chemical 'omics' approaches for understanding protein cysteine oxidation in biology. *Curr. Opin. Chem. Biol.* **15**, 88–102 (2011).
4. Guéraud, F. *et al.* Chemistry and biochemistry of lipid peroxidation products. *Free Radic. Res.* **44**, 1098–1124 (2010).
5. Fritz, K.S. & Petersen, D.R. An overview of the chemistry and biology of reactive aldehydes. *Free Radic. Biol. Med.* **59**, 85–91 (2013).
6. Rudolph, T.K. & Freeman, B.A. Transduction of redox signaling by electrophile-protein reactions. *Sci. Signal.* **2**, re7 (2009).
7. Fritz, K.S. & Petersen, D.R. Exploring the biology of lipid peroxidation-derived protein carbonylation. *Chem. Res. Toxicol.* **24**, 1411–1419 (2011).
8. Leonarduzzi, G., Robbesyn, F. & Poli, G. Signaling kinases modulated by 4-hydroxynonenal. *Free Radic. Biol. Med.* **37**, 1694–1702 (2004).
9. Jacobs, A.T. & Marnett, L.J. Heat shock factor 1 attenuates 4-Hydroxynonenal-mediated apoptosis: critical role for heat shock protein 70 induction and stabilization of Bcl-XL. *J. Biol. Chem.* **282**, 33412–33420 (2007).
10. Surh, Y.J. *et al.* 15-Deoxy-Δ12,14-prostaglandin J_2, an electrophilic lipid mediator of anti-inflammatory and pro-resolving signaling. *Biochem. Pharmacol.* **82**, 1335–1351 (2011).
11. Chipuk, J.E. *et al.* Sphingolipid metabolism cooperates with BAK and BAX to promote the mitochondrial pathway of apoptosis. *Cell* **148**, 988–1000 (2012).
12. Vila, A. *et al.* Identification of protein targets of 4-hydroxynonenal using click chemistry for *ex vivo* biotinylation of azido and alkynyl derivatives. *Chem. Res. Toxicol.* **21**, 432–444 (2008).
13. Codreanu, S.G., Zhang, B., Sobecki, S.M., Billheimer, D.D. & Liebler, D.C. Global analysis of protein damage by the lipid electrophile 4-hydroxy-2-nonenal. *Mol. Cell. Proteomics* **8**, 670–680 (2009).
14. Han, B., Hare, M., Wickramasekara, S., Fang, Y. & Maier, C.S. A comparative 'bottom up' proteomics strategy for the site-specific identification and quantification of protein modifications by electrophilic lipids. *J. Proteomics* **75**, 5724–5733 (2012).
15. Roe, M.R., Xie, H., Bandhakavi, S. & Griffin, T.J. Proteomic mapping of 4-hydroxynonenal protein modification sites by solid-phase hydrazide chemistry and mass spectrometry. *Anal. Chem.* **79**, 3747–3756 (2007).
16. Kim, H.Y., Tallman, K.A., Liebler, D.C. & Porter, N.A. An azido-biotin reagent for use in the isolation of protein adducts of lipid-derived electrophiles by streptavidin catch and photorelease. *Mol. Cell Proteomics* **8**, 2080–2089 (2009).
17. Aldini, G. *et al.* Identification of actin as a 15-deoxy-Δ12,14-prostaglandin J_2 target in neuroblastoma cells: mass spectrometric, computational, and functional approaches to investigate the effect on cytoskeletal derangement. *Biochemistry* **46**, 2707–2718 (2007).
18. Shearn, C.T., Fritz, K.S., Reigan, P. & Petersen, D.R. Modification of Akt2 by 4-hydroxynonenal inhibits insulin-dependent Akt signaling in HepG2 cells. *Biochemistry* **50**, 3984–3996 (2011).

19. Bennaars-Eiden, A. *et al.* Covalent modification of epithelial fatty acid-binding protein by 4-hydroxynonenal *in vitro* and *in vivo*. *J. Biol. Chem.* **277**, 50693–50702 (2002).
20. Higdon, A.N. *et al.* Methods for imaging and detecting modification of proteins by reactive lipid species. *Free Radic. Biol. Med.* **47**, 201–212 (2009).
21. LoPachin, R.M., Gavin, T., Petersen, D.R. & Barber, D.S. Molecular mechanisms of 4-hydroxy-2-nonenal and acrolein toxicity: nucleophilic targets and adduct formation. *Chem. Res. Toxicol.* **22**, 1499–1508 (2009).
22. Doorn, J.A. & Petersen, D.R. Covalent modification of amino acid nucleophiles by the lipid peroxidation products 4-hydroxy-2-nonenal and 4-oxo-2-nonenal. *Chem. Res. Toxicol.* **15**, 1445–1450 (2002).
23. Weerapana, E. *et al.* Quantitative reactivity profiling predicts functional cysteines in proteomes. *Nature* **468**, 790–795 (2010).
24. Rostovtsev, V.V., Green, J.G., Fokin, V.V. & Sharpless, K.B. A stepwise Huisgen cycloaddition process: copper(I)-catalyzed regioselective "ligation" of azides and terminal alkynes. *Angew. Chem. Int. Edn Engl.* **41**, 2596–2599 (2002).
25. Yang, J.J. *et al.* ZAK inhibits human lung cancer cell growth via ERK and JNK activation in an AP-1-dependent manner. *Cancer Sci.* **101**, 1374–1381 (2010).
26. Bloem, L.J. *et al.* Tissue distribution and functional expression of a cDNA encoding a novel mixed lineage kinase. *J. Mol. Cell Cardiol.* **33**, 1739–1750 (2001).
27. Wong, J. *et al.* Small molecule kinase inhibitors block the ZAK-dependent inflammatory effects of doxorubicin. *Cancer Biol. Ther.* **14**, 56–63 (2013).
28. Wang, X. *et al.* Complete inhibition of anisomycin and UV radiation but not cytokine induced JNK and p38 activation by an aryl-substituted dihydropyrrolopyrazole quinoline and mixed lineage kinase 7 small interfering RNA. *J. Biol. Chem.* **280**, 19298–19305 (2005).
29. Yu, X. & Bloem, L.J. Effect of C-terminal truncations on MLK7 catalytic activity and JNK activation. *Biochem. Biophys. Res. Commun.* **310**, 452–457 (2003).
30. Bachovchin, D.A. *et al.* Academic cross-fertilization by public screening yields a remarkable class of protein phosphatase methylesterase-1 inhibitors. *Proc. Natl. Acad. Sci. USA* **108**, 6811–6816 (2011).
31. Patricelli, M.P. *et al.* Functional interrogation of the kinome using nucleotide acyl phosphates. *Biochemistry* **46**, 350–358 (2007).
32. Shen, H.M. & Liu, Z.G. JNK signaling pathway is a key modulator in cell death mediated by reactive oxygen and nitrogen species. *Free Radic. Biol. Med.* **40**, 928–939 (2006).
33. Uchida, K. 4-Hydroxy-2-nonenal: a product and mediator of oxidative stress. *Prog. Lipid Res.* **42**, 318–343 (2003).
34. Dubinina, E.E. & Dadali, V.A. Role of 4-hydroxy-trans-2-nonenal in cell functions. *Biochemistry (Mosc.)* **75**, 1069–1087 (2010).
35. Liu, Q. *et al.* Developing irreversible inhibitors of the protein kinase cysteinome. *Chem. Biol.* **20**, 146–159 (2013).
36. Huang, X. *et al.* Crystal structure of an inactive Akt2 kinase domain. *Structure* **11**, 21–30 (2003).
37. Wang, T., Kartika, R. & Spiegel, D.A. Exploring post-translational arginine modification using chemically synthesized methylglyoxal hydroimidazolones. *J. Am. Chem. Soc.* **134**, 8958–8967 (2012).
38. Weerapana, E., Simon, G.M. & Cravatt, B.F. Disparate proteome reactivity profiles of carbon electrophiles. *Nat. Chem. Biol.* **4**, 405–407 (2008).
39. Ban, H., Gavrilyuk, J. & Barbas, C.F. III. Tyrosine bioconjugation through aqueous ene-type reactions: a click-like reaction for tyrosine. *J. Am. Chem. Soc.* **132**, 1523–1525 (2010).

ONLINE METHODS

Preparation of human cancer cell line proteomes. MDA-MB-231 cells (from ATCC) were grown in L15 medium supplemented with 10% FBS at 37 °C in a CO_2-free incubator. For *in vitro* labeling experiments, cells were grown to 100% confluency, washed three times with PBS and scraped in cold PBS. Ramos cells (from ATCC) were grown in RPMI medium supplemented with 10% FBS at 37 °C in a 5% CO_2 incubator, and cells were harvested at a density of 10^6 cells/mL. Cell lines were confirmed to be negative for mycoplasma contamination at the time of acquisition and were frozen at early passages before expansion and use. MDA-MB-231 and Ramos cell pellets were isolated by centrifugation at 1,400*g* for 3 min, and the cell pellets were stored at −80 °C until further use. The harvested cell pellets were lysed by sonication in PBS buffer and fractionated by centrifugation (100,000*g*, 45 min) to yield soluble and membrane proteomes. The proteomes were prepared fresh from the frozen cell pallets before each experiment.

***In vitro* LDE treatment.** HNE was purchased from EMD Biosciences, 15d-PGJ2 was purchased from Cayman Chemicals and 2-HD was purchased from Santa Cruz Biotechnology. Proteome samples were diluted to a 4 mg protein/mL solution in PBS. For each profiling experiment, one aliquot of the proteome sample (0.5 mL) was treated with 100 μM of LDE using 5 μL of a 10 mM stock, and the other aliquot was treated with 5 μL of either ethanol (for HNE and 15d-PGJ2) or DMSO (for 2-HD) as control. Samples were prepared in at least four replicates for each proteome-LDE combination. For the concentration-dependent profiling experiments using HNE, aliquots of the proteomes (0.5 mL each) were treated with 5, 10, 50, 100 and 500 μM of HNE using 5 μL of 0.5, 1.0, 5, 10 and 50 mM of stock solution, respectively. After 60 min of treatment at room temperature, both the LDE-treated and control aliquots were passed through a NAP-5 Sephadex column (GE Healthcare) to remove any unreacted LDE. The volume of each aliquot was increased to 1 mL with the concentration at 2 mg/mL after this step.

***In situ* HNE treatment.** After MDA-MB-231 cells were grown to 100% confluency, the medium was removed and replaced with fresh serum-free medium containing 50 or 100 μM HNE (10 or 20 μL of 50 mM stock in ethanol in 10 mL of medium). A control flask of cells was treated with 10 mL of serum-free medium containing 10 or 20 μL of ethanol in parallel. The cells were incubated at 37 °C for 1 h and harvested as detailed above to prepare HNE-treated and control proteomes, respectively. Samples were prepared in duplicate.

Protein labeling and click chemistry. Each of the control and LDE-treated proteome samples (~2 mg protein/mL in 1-mL volume) was treated with 100 μM of IA probe using 10 μL of a 10 mM stock in DMSO. The labeling reactions were incubated at room temperature for 1 h. Click chemistry was performed by the addition of 100 μM of either the heavy-TEV-tag (for the control sample) or light-TEV-tag (for the LDE-treated sample) (20 μL of a 5 mM stock), 1 mM TCEP (fresh 50× stock in water), 100 μM ligand (17× stock in DMSO:*t*-butanol 1:4) and 1 mM $CuSO_4$ (50× stock in water). Samples were allowed to react at room temperature for 1 h. After the click chemistry step, the light- and heavy-labeled samples were centrifuged (5,900*g*, 4 min, 4 °C) to pellet the precipitated proteins. The pellets were mixed together and washed twice in cold MeOH, after which the pellet was solubilized in PBS containing 1.2% SDS via sonication and heating (5 min, 80 °C). Samples were subjected to streptavidin enrichment of probe-labeled proteins, sequential on-bead trypsin and TEV digestion, and liquid chromatography–tandem mass spectrometry (LC-MS/MS) analysis according to the published isoTOP-ABPP protocol[23].

MS data analysis. For each LC-MS/MS run, IA probe–labeled peptides were identified by Sequest[40] and DTASelect[41], and the quantification of heavy/light ratios (isoTOP-ABPP ratios, *R*) was performed by an in-house software (CIMAGE) as previously described[23] (available upon request). The software was advanced to be able to detect and quantify cases where near-complete LDE blockade of IA-probe labeling was achieved (for example, very small or no light peak) and assign an empirical ratio cutoff of 15 to each of such cases. After ratios for unique peptides were calculated for each run, overlapping peptides with the same labeled cysteine (for example, same local sequence around the labeled cysteines but different charge states, MudPIT segment numbers, or tryptic termini) were grouped together (as a 'peptide entry'), and the median ratio from each group was recorded as the *R* ratio of this peptide entry in this run.

For the *in vitro* profiling with three different LDEs, each experiment (one proteome-LDE combination) contained at least four replicate runs. The *R* ratios of each peptide entry from multiple replicate runs were averaged, and the mean value was reported as its final *R* ratio in this experiment. Cases were excluded from further analysis when large variability in *R* ratios across multiple replicate runs were observed (s.d. >2/3 of the mean) or when *R* ratios were not quantified in two or more replicate runs for any of the six proteome-LDE experiments.

For the *in vitro* profiling with HNE competition at different concentrations, all runs were searched using Sequest and filtered with DTASelect as described above. Because the mass spectrometer was configured for data-dependent fragmentation, peptides are not always identified in every run. In the case of probe-modified peptides that were sequenced in one but not the other runs, a featured algorithm of CIMAGE was used to identify the corresponding peak pairs in the runs without the Sequest identification and obtain quantification as previously described.

For the *in situ* profiling with HNE at 50 and 100 μM, two replicate samples were prepared for each condition (four runs in total). Peptide entries without quantified ratios from at least two runs (either two different concentrations or two replicates at the same HNE concentration) were removed from further analysis.

In all cases, the false positive rate after quantification was found to be less than 1%. All of these values can be found in **Supplementary Tables 1**, **3** and **4**.

All RAW data and DTASelect files have been deposited in PeptideAtlas under accession number PASS00353.

Retroviral overexpression of Flag-tagged ZAK proteins in HEK-293T cells. Full-length cDNA encoding human ZAK-β (BC001401) in pOTB7 was purchased from Open BioSystems and subcloned into pFLAG-CMV-6c (Sigma-Aldrich). ZAK-C22A and ZAK-K45M mutants were generated by QuikChange site-directed mutagenesis using the primer

doi:10.1038/nmeth.2759

5′-atttgatgacttgcagttttttgaaaacgccggtggaggaagttttg- 3′ and 5′-ggac aaggaggtggctgtaatgaagctcctcaaaatagag-3′ and their complements. Wild-type and mutant ZAK were cloned into a modified pCLNCX retroviral vector. Retrovirus was prepared by taking 3.0 μg of each of pCLNCX and pCL-Ampho vectors and 18 μL of FuGENE HD reagent (Roche) to transfect 60%-confluent HEK-293T cells. Medium was replaced after 1 d of transfection, and the next day virus-containing supernatant was collected, filter sterilized and stored at −70 °C. 1 mL of virus-containing medium was used to infect target cells in the presence of 8 μg/mL of polybrene for 72 h, and infected cells were selected in medium containing 100 μg/mL of hygromycin. Surviving cells after the selection were expanded and cultured in regular DMEM medium with 10% FCS.

Immunoprecipitation of Flag-tagged ZAK proteins. HEK-293T cells with stable expression of wild-type or mutant ZAK were grown to 100% confluency on a 10-cm plate. Cells were collected, washed twice with 10 mL of cold PBS (2 × 10 mL) and lysed in 1 mL of PBS supplemented with 1× Complete EDTA-free protease inhibitor cocktails by sonication. Cell lysates were fractionated by centrifugation (100,000*g*, 45 min), and the soluble fraction was incubated with 50 μL of anti-Flag M2 affinity gel (Sigma-Aldrich) at 4 °C for 3 h. Beads were washed with 5 × 1 mL of cold PBS (10 min per incubation), and Flag-tagged ZAK was eluted by either 150 μg/mL of 3×Flag-peptide solution provided by the manufacturer or by 4× gel loading buffer, depending on the downstream applications.

In-gel fluorescence characterization of ZAK labeled by IA probe. Flag-tagged wild-type and C22A mutant ZAK were immunoprecipitated from HEK-293T cells (10^7 cells). After washing with PBS, the beads were suspended in 100 μL of PBS buffer and labeled with 250 nM of IA-rhodamine (by addition of 1 μL of 25 μM probe stock in DMSO). After 1 h of labeling at 4 °C, 50 μL of 4× gel loading buffer was added, and the beads were boiled for 5 min to elute the bound proteins. Gel samples were separated by SDS-PAGE (50 μL of sample per lane) and visualized in-gel using a Hitachi FMBio II flatbed laser-induced fluorescence scanner (MiraiBio). For testing HNE blockade on IA labeling of ZAK by gel, soluble lysate of HEK-293T overexpressing WT ZAK was incubated with 10, 50 and 100 μM of HNE (by addition of 2 μL of 5, 25 and 50 mM stock) for 30 min and then subjected to immunoprecipitation.

In-gel fluorescence characterization of ZAK labeled by HNEyne probe. 50 μL of soluble lysate (1 mg/mL in PBS) of HEK-293T cells transfected with mock, ZAK-WT and ZAK-C22A was labeled with 10 μM of HNEyne[12] (Cayman Chemicals, 1 μL of 500 μM stock in ethanol) for 1 h at room temperature. Cycloaddition was performed with 200 μM rhodamine-azide, 1 mM TCEP, 100 μM TBTA ligand and 1 mM $CuSO_4$. The reaction was allowed to proceed at room temperature for 1 h before quenching with 20 μL of 4× SDS-PAGE loading buffer (reducing). Quenched reactions were separated by SDS-PAGE (40 μL of sample per lane) and visualized in-gel using a fluorescence scanner. For the *in situ* HNEyne labeling, WT and C22A ZAK–transfected cells were grown in a six-well plate to 100% confluency and switched into 1 mL of serum-free DMEM medium. Cells were labeled with 5 μM of HNEyne probe (1 μL of 5 mM stock) for 1 h at 37 °C. Cells were then harvested, washed with cold PBS and lysed in 200 μL of PBS with protease inhibitors. 50 μL of soluble lysates were subjected to the cycloaddition protocol as described above, and probe labeling was monitored by in-gel fluorescence.

ZAK *in vitro* kinase activity assay. The kinase activity assay protocol was adapted from that of Yu and Bloem[29]. Kinase assay buffers, myelin basic protein (MBP) substrate and ATP stock solution were purchased from SignalChem. Radio-labeled [^{33}P]ATP was purchased from PerkinElmer. 10 mg of soluble lysate of HEK-293T cells transfected with each of WT, C22A and K45M ZAK was immunoprecipitated and then eluted with 2 × 300 μL 3×Flag-peptide buffer. Each sample was concentrated to 100 μL using an Amicon centrifugal filter (30-kDa cutoff) and exchanged to the assay kinase buffer (5 mM MOPS, pH 7.2, 2.5 mM β-glycerol-phosphate, 5 mM $MgCl_2$, 1 mM EGTA, 0.4 mM EDTA, 0.05 mM DTT and 40 ng/μL BSA) to a final volume around 10 μL. For each ZAK construct, four reactions were set up, and each reaction started with mixing 10 μL of immunoprecipitated ZAK, 5 μL of MBP (1 mg/mL) and 5 μL of HNE (10 or 100 μM) or H_2O together. No-enzyme and no-substrate controls were prepared in parallel. The mixed samples were incubated on ice for 15 min, and 5 μL of [^{33}P]-ATP assay cocktail (250 μM, 167 μCi/mL) was then added to initiate the kinase reaction. Each reaction mixture was incubated in 30 °C for 15 min, and the reaction was terminated by spotting 20 μL of the reaction mixture onto individual precut strips of phosphocellulose P81 paper. The spotted P81 strips were air dried and then washed with 10 mL of 1% phosphoric acid for 3 × 10 min. ZAK activity was measured by counting the radioactivity on the P81 paper in the presence of scintillation fluid in a scintillation counter after subtracting the value obtained from the corresponding no-substrate control, and all measured activities were normalized to that of ZAK-WT without HNE treatment. Experiments were performed in triplicates. 10 μL of each ZAK variant used in setting up the kinase reaction was run on a SDS-PAGE gel and immunoblotted with an anti-Flag antibody to ensure that they are enriched at similar levels (**Supplementary Fig. 4**).

Measurement of HNE blockade of ATP binding of ZAK by SILAC-ABPP. HEK-293T cells with stable expression of WT ZAK were passaged six times in DMEM medium minus L-lysine and L-arginine (Thermo) supplemented with 10% dialyzed FBS (Gemini), 1% PSQ (1% (vol/vol) 10,000 units penicillin, 10 mg streptomycin, 29.2 mg L-glutamate solution) and 100 μg/mL [$^{13}C_6$, $^{15}N_4$]L-arginine–HCl and [$^{13}C_6$,$^{15}N_2$]L-lysine–HCl (heavy) or L-arginine–HCl and L-lysine–HCl (light) (Sigma-Aldrich). Soluble proteomes of light and heavy ZAK-WT–transfected HEK-293T cells (3 mL each at 9 mg/mL) were treated with 100 μM of HNE (6 μL of 50 mM stock) or DMSO for 30 min at room temperature, respectively. The proteomes were gel filtrated by PD-10 columns (GE Healthcare) to remove unreacted HNE and were split into four aliquots (0.5 mL, 6 mg/mL). Each of the four aliquots of light and heavy proteomes was labeled with 20 μM of acyl phosphate–ATP probe (ActivX Biosciences) for 10 min and then heavy and light proteomes mixed together to proceed with reduction/alkylation, streptavidin enrichment, and trypsin digest according to a modified version of the vendor-provided "Xsite Kinase Analysis" protocol[42]. The four trypsin-digested samples

were analyzed by LC-MS/MS, and enriched peptides were identified by Sequest and DTASelect. The amounts of probe-labeled ZAK and other proteins in the proteome with and without HNE treatment were quantified using the CIMAGE module that was developed for quantitative SILAC-ABPP[43]. Quantitation data from the four MS runs were combined, and peptides from keratin proteins and decoy proteins were removed. Cases were excluded from further analysis when proteins were not quantified in at least two out of the four runs and with at least three unique tryptic peptides, or when quantified with large variability across multiple runs (s.d. >2/3 of the mean). *R* ratios (DMSO-treated heavy versus HNE-treated light proteomes) of protein targets that passed the filter were plotted in **Figure 4e**. As an internal control, untreated and unenriched proteomes were digested with trypsin and analyzed by LC-MS/MS to quantify the relative levels of proteins in heavy and light amino acid–labeled cells. This control confirmed ZAK showed an *R* ratio of 0.62 (heavy/light), which was similar to the median ratio of 0.72 (heavy/light) quantified for all proteins. Quantified ratios from these SILAC-ABPP experiments are reported in **Supplementary Table 6**.

Western blotting of phospho-MAPKs in ZAK-transfected HEK-293T cells. Mouse and rabbit monoclonal antibodies against phospho-ERK 1/2 (Thr202/Tyr204), phospho-SAPK/JNK (Thr183/Thr185), phospho-p38 MAPK (Thr180/Thr182) and total ERK 1/2, SAPK/JNK and p38 MAPK were purchased from Cell Signaling Technology (catalog #9106, 9255, 9216, 9212, 9252, 4695). HEK-293T cells transfected with WT, C22A and K45M ZAK as well as mock-transfected cells were seeded into a 12-well plate with 2.5×10^5 cells per well. Cells were grown in regular DMEM medium with 10% FBS for 24 h and starved in serum-free DMEM medium for another 24 h. Cells were then treated at 37 °C either with 100 µM of HNE (2 µL of 50 mM stock) for 30 min followed by 1 mM of H_2O_2 for 30 min or with 50 or 100 µM of HNE alone for 60 min. After the treatment, cells were harvested, washed with 2 × 1 mL of cold PBS and then lysed by sonication in 100 µL of PBS buffer supplemented with 1× Complete protease inhibitors cocktail and 1× PhosSTOP phosphatase inhibitors cocktail (Roche). 30 µg of soluble lysate of each sample was separated by SDS-PAGE, transferred to a nitrocellulose membrane, blocked in 5% milk TBST and blotted against the primary antibodies (1:2,000) listed above for 16 h at 4 °C. After a washing step in TBST (3 × 10 min), membranes were blotted with IRDye secondary antibodies (1:10,000) for 1 h at room temperature and scanned by an Odyssey imaging system (LI-COR). Protein band intensities were quantified by ImageJ[44], and ratios of phosphor-MAPK over total MAPK were computed. Experiments were repeated in at least four replicates.

40. Eng, J.K., McCormack, A.L. & Yates, J.R. III. An approach to correlate tandem mass spectral data of peptides with amino acid sequences in a protein database. *J. Am. Soc. Mass Spectrom.* **5**, 976–989 (1994).
41. Cociorva, D., Tabb, D.L. & Yates, J.R. Validation of tandem mass spectrometry database search results using DTASelect. *Curr. Protoc. Bioinformatics* **16**, 13.4 (2007).
42. Patricelli, M.P. *et al.* *In situ* kinase profiling reveals functionally relevant properties of native kinases. *Chem. Biol.* **18**, 699–710 (2011).
43. Adibekian, A. *et al.* Click-generated triazole ureas as ultrapotent *in vivo*-active serine hydrolase inhibitors. *Nat. Chem. Biol.* **7**, 469–478 (2011).
44. Schneider, C.A., Rasband, W.S. & Eliceiri, K.W. NIH Image to ImageJ: 25 years of image analysis. *Nat. Methods* **9**, 671–675 (2012).

doi:10.1038/nmeth.2759